

Stochastic gravitational-wave background search using data from five pulsar timing arrays

Wang-Wei Yu * and Bruce Allen †

Max Planck Institute for Gravitational Physics (Albert Einstein Institute),
Leibniz Universität Hannover, Callinstrasse 38, D-30167, Hannover, Germany

(Dated: December 10, 2025)

Using public data from five pulsar timing arrays (PTAs), we search for a stationary, isotropic, and unpolarized nHz stochastic gravitational-wave background (SGWB). We use pulse-time-of-arrival data from 121 pulsars, which is more informative than previous searches, carried out separately by the individual PTA collaborations using only their own data. For pulsars observed by more than one PTA, we employ a new “direct combination” method to merge their astrophysical models and data. This avoids the challenge of reconciling the different PTA timing models to obtain a single “best” model. A central result of our analysis is posterior probability distributions for the amplitude A_{gw} and exponent γ_{gw} of the putative SGWB energy-density spectrum, modeled as a power law in frequency. While these results are consistent with a nonzero SGWB amplitude A_{gw} , the statistical significance—assessed via a Bayesian odds ratio and through noise-marginalized false-alarm probabilities (p -values) for three different detection statistics—remains below the conventional 5σ threshold for a confident detection. We also reconstruct the inter-pulsar timing-residual correlation, as a function of the angle θ between the pulsar lines of sight. This is consistent with the curve predicted by Hellings and Downs (HD).

Introduction – Pulsar timing arrays (PTAs) aim to detect low frequency gravitational waves (GWs), by searching for the effects that such waves induce on the arrival times of pulsar pulses. These GWs create “timing residuals” which are correlated among different pulsars [1, 2]. Decades-long datasets with submicrosecond timing precision yield GW amplitude (strain) sensitivities of order $A_{gw} \sim 10^{-15}$ at nHz frequencies.

Orbiting pairs of supermassive black holes (SMBHs) are one possible source of GWs. If the Universe contains many such pairs, then the incoherent superposition of their GW emissions would create a stochastic GW background (SGWB) [3–5] with a power-law spectrum in the nHz band.

Different PTA collaborations have reported varying levels of evidence for a nHz SGWB. The Parkes PTA (PPTA [6]) observed 30 pulsars over 18 years, concluding that the data showed “no support for or against”. The European and Indian PTAs (EPTA and InPTA [7]) observed 25 pulsars, and reported “marginal evidence” in the 25-year dataset and “evidence” when only the last 10 years of data were analyzed. The Chinese PTA (CPTA [8]) observed 57 pulsars over three years, and reported “some evidence”. The North American Nanohertz Observatory for Gravitational Waves (NG [9]) observed 67 pulsars over 15 years and reported “compelling evidence”. Most recently, the MeerKAT PTA (MPTA [10]) observed 83 pulsars over 4.5 years, and, depending on assumptions about pulsar noise processes, reported either “high significance” or “no significance” (also see [11]). None of these pass the threshold of 5σ significance required to claim detection [12].

All of these PTAs (apart from CPTA) have released their data to the public. Using this full public dataset

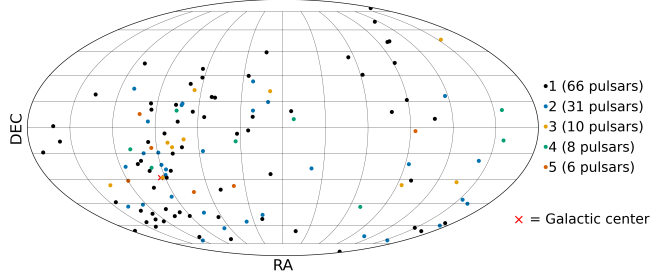


FIG. 1. A Mollweide projection showing sky locations of the 121 pulsars included in our analysis. Colors indicate how many PTAs contributed data for each pulsar.

increases the total number of distinct pulsars to $N = 121$, as shown in Fig. 1. PTAs search for an SGWB by correlating pairs of pulsars, whose number scales as N^2 . Furthermore, since most pulsars are observed by more than one collaboration, there are also more data samples per pulsar. Hence, analysis of the full dataset should significantly increase the GW strain sensitivity and the detection confidence [2, 13–15].

We analyze this five-PTA dataset [16–20] using a recently proposed “direct combination” method [21, 22]. This allows us to combine the data with only minor modifications, as described below. Tests of this method, carried out with the International Pulsar Timing Array (IPTA) Data Release 2 (DR2) combined data set from 2019 [14], suggest that it produces results that are identical to traditional (but more time-consuming) data combination techniques.

Aside from this, our analysis is standard. We use the same tools and methods as the individual PTAs, as implemented in `Enterprise` [23] and in the next-generation PTA data-analysis package `Discovery` [24]. Both are

based on parameterized likelihood models and employ Markov chain Monte Carlo methods. These produce posterior samples (here called “posteriors”) that approximate the inferred posterior probability distributions of the model parameters.

Methods, Models, and Conventions – Because we use standard methods, this paper is brief. When we follow the PTA analyses described above [6–10], we give only a brief description and cite the relevant literature. If we do something different, then more details are provided.

As is usual in this field, our analysis considers two alternative hypotheses or “models”:

- The *signal hypothesis*, denoted by “HD”, is a model with two contributions to the pulsar pulse arrival-time residuals. The first is pulsar noise, assumed to be (a) uncorrelated between pulsars and (b) a sum of stationary “red” (RN) and “dispersion measure” (DM) noise plus a nonstationary “white noise” (WN) component. The second contribution arises from a stationary, unpolarized and isotropic SGWB, as described by the general theory of relativity (GR). This SGWB component, determined by parameters A_{gw} and γ_{gw} defined below, induces timing-residual correlations between pulsar pairs, which are assumed to follow the Hellings and Downs (HD) prediction [2, 25, 26] given in (2). Both contributions are assumed to arise from (the sum of) many independent sources; by the central limit theorem, the resulting timing residuals form a zero-mean Gaussian process, which is fully characterized by its covariance matrix \mathbf{C} .
- The *null hypothesis* is called “common uncorrelated red noise” and is denoted by CURN. Again, the timing residuals are assumed to be drawn from a zero-mean Gaussian process, but this time entirely characterized by the covariance matrix $\mathbf{C}_0 = \text{diag } \mathbf{C}$. Since our null hypothesis *is defined via our signal hypothesis*, it has *exactly* the same parameters/noise-models as the signal hypothesis.

The diagonal operation sets to zero all elements where the row and column have different pulsars, eliminating the HD correlations [27]. It does *not* remove the dependence upon A_{gw} and γ_{gw} , which also enter via the diagonal terms. Thus, CURN does not correspond to the *absence* of GWs, but rather to “GWs” which create arrival-time fluctuations *lacking* the inter-pulsar correlations predicted by GR. Alternatively, CURN corresponds to an astrophysical or nuclear/QCD physics process of unknown origin, generating Gaussian rotational fluctuations which are uncorrelated between pulsars, but have the exact same power-law spectrum for all pulsars [2]. CURN is considered a more conservative null hypothesis than that of “no GWs”.

Using *Discovery* [24] as a tool, and conditioning the Gaussian likelihood on the data and the priors, we generate posteriors for the HD and CURN models. These are

sets of parameter values that are most the consistent with the data and priors; they characterize the joint posterior probability distributions of the model parameters.

For this work, the most important model parameters are the amplitude A_{gw} and exponent γ_{gw} of the SGWB power-law power spectrum. To define these, let $d\rho_{gw}$ denote the SGWB energy density in the frequency range $[f, f + df]$ and let $\rho_{cr} = 3c^2H_0^2/8\pi G \simeq 7.7 \times 10^{-10} \text{ J/m}^3$ denote the critical (closure) energy density of the Universe. Here, c is the speed of light, G is Newton’s gravitational constant, and $H_0 \simeq 67.4 \text{ km/s Mpc} \simeq 2.2 \times 10^{-18} \text{ Hz}$ is the current Hubble expansion rate. Then

$$\Omega_{gw}(f) \equiv \frac{f}{\rho_{cr}} \frac{d\rho_{gw}}{df} = \frac{2\pi^2}{3H_0^2} A_{gw}^2 f_r^2 \left(\frac{f}{f_r}\right)^{-\gamma_{gw}+5}, \quad (1)$$

where $f_r = 1/\text{yr} \simeq 31.7 \text{ nHz}$ is a standard reference frequency. Together with our previous assumptions, this spectral model (assumed to apply in the range $2 < f/\text{nHz} < 200$) fully characterizes the SGWB.

One result of this analysis is posterior probability distributions for A_{gw} and γ_{gw} . We consider models in which γ_{gw} is free, and those where it is constrained to take the value 13/3. The latter would be expected from a population of SMBHs in circular binaries, provided that GWs dominate the energy loss at nHz frequencies.

One way to assess detection confidence is via frequentist detection statistics [27]. We present results for three different statistics that are used within the PTA community. All three statistics D are quadratic functions of the timing residuals, with weights determined by \mathbf{C} and \mathbf{C}_0 .

Each of the posteriors corresponds to a different model universe, with its own amplitudes and exponents for the different noise sources, and thus with its own covariance matrices \mathbf{C} and \mathbf{C}_0 . This means that the values of the detection statistics D , and the probability (*p*-value) of obtaining them under CURN, differ from one posterior sample to the next. Thus, to assess detection confidence, we present the posterior distributions of these *p*-values. In the literature, its mean is called the “noise-marginalized false-alarm probability” [28] or “posterior predictive *p*-value” [29].

Some past work uses ad-hoc methods for assessing the false-alarm probability *p*. “Sky scrambling” and “phase shifting” were intended to “remove any signal from the data”. The first leaves the data invariant but assigns a large number of random sky positions to the different pulsars, thus destroying the HD correlation [30, 31]. The second retains the pulsar’s positions, but randomizes the phases of the (frequency-domain Fourier amplitudes of the) data [31]. However, neither of these methods properly reproduces the null distribution of D [32]. For example, because phase shifting does not modify the squared modulus of the Fourier amplitudes, it introduces less variance in D than would arise under the null hypothesis.

We determine the false-alarm probability *p* using a correct method [27, 32–34]. Since D is a quadratic form in

the data, its distribution under CURN is a generalized χ^2 distribution [27, 32, 33]; the probability that it exceeds the observed value in one of our posterior samples is found analytically.

To aid interpretation, we also report the p -values as “equivalent $q\sigma$ ” levels: $q > 0$ is chosen so that a random draw from a zero-mean Gaussian with variance σ^2 has probability p of exceeding $q\sigma$. This “one-sided p value” satisfies $2p = \text{erfc}(q/\sqrt{2})$. For example, 1σ corresponds to $p = 16\%$, 2σ corresponds to $p = 2.3\%$, 3σ corresponds to $p = 0.14\%$, 4σ corresponds to $p = 3.2 \times 10^{-5}$, and 5σ corresponds to $p = 2.9 \times 10^{-7}$. The latter, a false-alarm probability of less than one per three million, is the traditional threshold for confident detection [12].

Analysis of the five-PTA dataset – The data from the five PTAs come from 121 millisecond pulsars, as shown in Fig. 1. These consist of the second EPTA data release (10-year subset) [16, 35], the first InPTA data release [17, 36], the MPTA 4.5-yr data release [18, 37], the NG 15yr data release [19, 38], and the third PPTA data release [20, 39]. Each PTA’s data consists of one `.par` file and one or more `.tim` files, per pulsar.

We merge these using the direct combination method [21, 22]. The `.tim` files, containing pulse times-of-arrival (TOAs) and their uncertainties, are used “as is”. The `.par` files, containing the astrophysical models, and some detector-specific parameters, are modified (in effect) as follows, one pulsar at a time. (This is also the first step of “manual” data combination.)

1. For pulsars observed by more than one PTA, a “reference PTA” is selected via the arbitrary ordering NG > EPTA > PPTA > MPTA. (InPTA is not listed because its pulsars are observed by other PTAs.) Any *other* PTAs that have data for this pulsar are called “target PTAs”.
2. Since some pulsars have both J- and B-style names, the name is copied from the reference `.par` file to the target `.par` files.
3. Any `.par` file that uses the TCB time standard is converted to TDB using `Tempo2` [40] tools.
4. If the reference `.par` file has a DMX model for DM fluctuations (NG and InPTA only), then it is replaced by a Gaussian process (DMGP) model. The parameter DM0 is initialized to the mean DMX value, and DM1 and DM2 are initialized to zero.
5. If the reference `.par` file has a DMGP model, then the DM0 value is retained, and DM1 and DM2 are initialized to zero.
6. The astrophysical model β [1, Eq. 7.2], including sky position, proper motion, spin frequency, spin-down parameters, binary orbital parameters, and DM values, is copied from the reference `.par` file to the target `.par` files.

Detector-specific parameters in the `.par` files, for example, “JUMP” for time offsets and “FDx” for narrow-band frequency offsets, are unchanged. This allows for template model shape differences between PTAs.

For four pulsars, ad-hoc “tricks” are used to maintain phase connection between the `.tim` file TOAs. For the binary pulsar PSR J2241-5236 (MPTA, PPTA), we retain the MPTA 11-parameter model and the PPTA 18-parameter model for the orbital frequency evolution. The other parameters follow 6 above. For PSR J0610-2100 (MPTA, NG) and PSR J1024-0719 (EPTA, MPTA, NG, PPTA), we keep the DMX model for the NG data and the DMGP model for the remaining PTAs. For PSR J1804-2858 (MPTA), we retain the values of DM1 and DM2 rather than initializing them to zero.

The direct combination method [21, 22] works because the only significant change it makes is to the parameters β , item 6 above. While their exact values are unknown, every pulsar has *unique* values for these parameters, for example, the sky position. Those enter the analysis via a nominal value β_0 [1, Eq. 7.2] and via a matrix \mathbf{M} [1, Eq. 7.4], which is the rate of change of the pulse arrival-time with respect to variations ϵ in β . In the (tiny) region of interest, \mathbf{M} varies slowly with those parameters, so computing \mathbf{M} with the same β_0 for a given pulsar in all PTAs introduces negligible errors. The subsequent marginalization over $\epsilon = \beta - \beta_0$ [1, Eq. 7.6] fully accounts for the uncertainties in β and for the variations in its nominal value across PTAs. Similarly, the RN and DM noise are intrinsic to the pulsar and to the interstellar medium (ISM), so must be the same for all PTAs.

The next analysis step is single-pulsar noise modeling. The goal is to determine each pulsar’s WN covariance matrix \mathbf{N} , which appears in the Gaussian likelihood [1, Eq. 7.27]. This characterizes the timing residuals fluctuations which remain after subtracting the deterministic timing model determined by β , and stationary power-law-spectrum models for the RN and DM noise [1, Eq. 7.2, 7.26]. Note that the WN model is nonstationary: for a given pulsar/backend/PTA, the WN variance differs between observations.

Single-pulsar noise modeling determines two or three parameters per pulsar and backend. The WN covariance matrix \mathbf{N} is set by these parameters and by the `.tim` file contents. NG, PPTA, MPTA, and seven EPTA backends use the parameters *EFAC*, *EQUAD*, and *ECORR* [38, Eq. 2]. InPTA and the remaining EPTA backends only use *EFAC* and *EQUAD* [41].

The WN parameters for a given pulsar are obtained from *all* of its TOA data (meaning, all `.tim` files). These are analyzed using `JAXopt` [42], with priors taken from the Table I rows with an “S” in the final column; the amplitude and exponent priors are used for all power laws. For $\gamma < 7$, the $f \rightarrow 0$ divergences are absorbed by the timing model; for $\gamma > 1$, the $f \rightarrow \infty$ divergences are absent [43, 44]. Note that *EQUAD* has the units used

Parameters	Uniform on range	Stage
EFAC	(0.01, 10)	S
\log_{10} EQUAD	(-8.5, -5)	S
\log_{10} ECORR	(-8.5, -5)	S
γ	(1,7)	S, F
$\log_{10} A$	(-20, -11)	S, F

TABLE I. Priors for the WN parameters, and for the amplitudes/exponents of the power-law RN, DM and SGWB noise spectra. “S” denotes single pulsar, and “F” denotes full PTA.

in **Tempo** [45], **Tempo2** [40] and **PINT** [46], and is often written as *T2EQUAD*. The output is a “WN dictionary” of best-fit *EFAC*, *EQUAD* and (potentially) *ECORR* values, which are used in subsequent analysis to obtain \mathbf{N} [38, Eq. 2].

For pulsars with data from multiple PTAs, the WN parameters are shifted away from their single-PTA-analysis values. This is because the combined data allow better modeling of the low-frequency RN and DM noise, leading to more reliable estimates of the WN parameters.

We drop TOAs for any backends which have $EFAC < 0.1$ or $EFAC > 10$, since this indicates that the backend or template matching was unstable, or that RFI or calibration or instrumental issues were present. This removes 0.17% of the TOAs. Our final data for analysis comes from 25 EPTA pulsars, 13 (of 14) InPTA pulsars, 83 MPTA pulsars, 68 NG pulsars, and 31 (of 32) PPTA pulsars. (Data from InPTA pulsar J1022+1001 are dropped because all the *EFACs* are larger than 10. Data from PPTA pulsar PSR J1741+1351 are dropped because there were only 16 observations.)

The final stage is multi-pulsar analysis, following the procedures described in [1, 9]. We use both **Enterprise** [23] and the next generation PTA data-analysis package, **Discovery**, which is optimized via JAX for graphics processing units (GPU) [47]. The use of **Discovery** has significantly sped up our analysis.

Within the **Discovery** framework, we use the priors listed in Tab. I with an “F” in the final column. As described above, we consider two priors for the SGWB power-law power-spectrum exponent γ_{gw} . One is the uniform range given in Tab. I, the other is fixed to $\gamma_{gw} = 13/3$. Our analysis uses the Hamiltonian No-U-Turn Sampler (NUTS) [48, 49], as implemented in NumPyro [50–52]. NUTS is the default for **Discovery** [24], which provides the log-likelihood gradients needed by Hamiltonian samplers. It is much faster than the PTMCMC sampler [53] used by the individual PTAs when they analyzed their own data.

We generated 20480 posterior samples under the HD signal hypothesis, and the same number of posteriors under the CURN hypothesis. Each gives the amplitudes and exponents of the power-law models describing the pulsar (red and DM) noise, and the SGWB. We use these to evaluate the frequentist detection statistics and

their corresponding false-alarm probabilities (*p*-values) for each posterior sample.

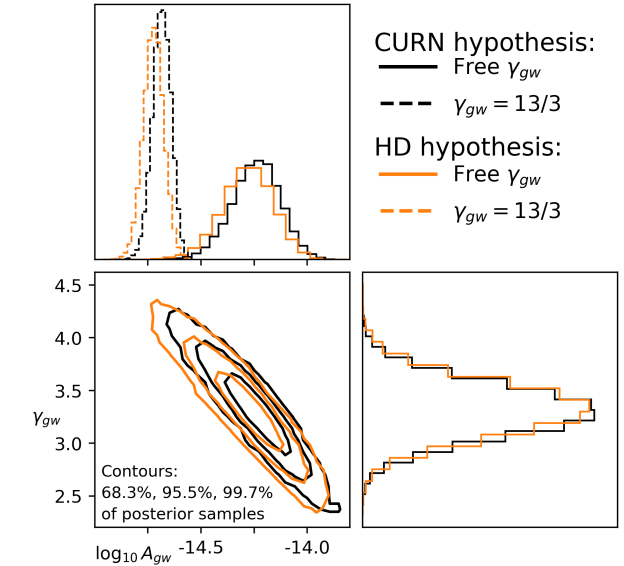


FIG. 2. The posteriors for the amplitude and exponent of the SGWB power spectrum, as defined in (1).

Results of the five-PTA analysis – One important result of this analysis are the posterior distributions of the SGWB power-spectrum amplitude A_{gw} and exponent γ_{gw} as defined in (1). These are shown in Fig. 2. The amplitude posterior is sharply peaked away from zero, which is consistent with (or evidence for) the presence of an SGWB. As expected, the posteriors are very similar for the two hypotheses. This is because, if there are $\lesssim 1500$ pulsars (see [54, Fig. 10]), most of the SGWB evidence arises from autocorrelations rather than cross-correlations—and by construction, CURN includes these autocorrelations.

Model	$\log_{10} A_{gw}$	γ_{gw}
CURN with free γ_{gw}	$-14.24^{+0.11}_{-0.11}$	$3.30^{+0.28}_{-0.27}$
CURN with $\gamma_{gw} = 13/3$	$-14.69^{+0.04}_{-0.04}$	
HD with free γ_{gw}	$-14.28^{+0.12}_{-0.12}$	$3.32^{+0.28}_{-0.28}$
HD with $\gamma_{gw} = 13/3$	$-14.72^{+0.05}_{-0.05}$	

TABLE II. Median posteriors values for A_{gw} and γ_{gw} , and their 68% containment intervals (gray bands in Fig. 3).

Happily, these posteriors, summarized in Table II, are consistent with the individual PTA results [6, 7, 9, 10]. They are more constraining than the posteriors obtained by the individual PTAs: the uncertainty ellipses in the bottom-left plot of Fig. 2 are smaller than those obtained by intersecting the individual PTA posteriors [55]. For example, the area = $\int d\gamma_{gw} \int d\log_{10}(A_{gw})$ of our 95.5% containment ellipse (for the HD hypothesis) is 45% of that shown in [55, Fig. 1, right]. As explained earlier, this is as expected for an SGWB: joint analysis yields more

evidence and is more constraining than naive intersection of the separate PTA results.

To claim an SGWB detection, there are several hurdles to overcome [12]. One must show that the data is consistent with the HD signal hypothesis, and that it is very unlikely (at the 5σ level) to arise under the CURN hypothesis. Clearly, the estimates of A_{GW} and γ_{GW} cannot help with this, since they are almost identical under both hypotheses.

One way to assess significance is through *null-hypothesis testing* [56] using a frequentist statistic. We use quadratic statistics of the form $D(z) = z^T \mathbf{Q} z$, where z is the data column vector, and consider three choices of the square *filter matrix* \mathbf{Q} (see [27, Eq. (1)]). The optimal statistic (OS) selects \mathbf{Q} to maximize the signal-to-noise ratio (SNR) [28]. The Neyman–Pearson (NP) statistic selects \mathbf{Q} to maximize the detection probability at fixed false-alarm probability p . The NP minimum-variance (NPMV) statistic adopts the NP matrix but sets all diagonal entries of \mathbf{Q} to zero, eliminating autocorrelation contributions.

Normally, the NP statistic would be preferred. However, because its filter matrix \mathbf{Q} contains both diagonal (autocorrelation) and off-diagonal (cross-correlation) terms, it is not robust against errors in modeling pulsar noise. In contrast, the OS and NPMV statistics use filter matrices that contain only off-diagonal terms, making them more robust. Details may be found in [27].

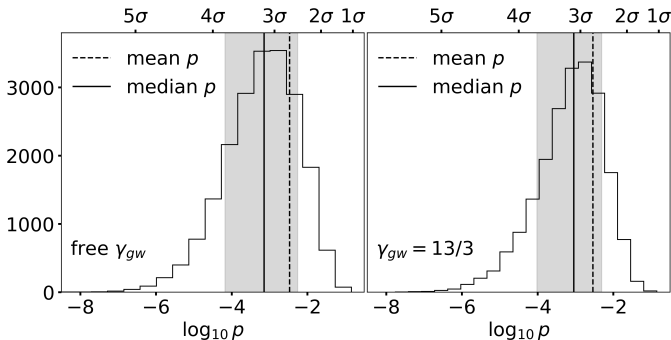


FIG. 3. Histograms of NPMV detection statistic p -values for the 20480 CURN-hypothesis posterior samples. The left panel has γ_{gw} free, and the right has $\gamma_{gw} = 13/3$. The upper horizontal axis is one-sided-Gaussian equivalent significance.

The values of these statistics and their false-alarm probabilities p depend on the observational data and on the (inferred) pulsar-noise models under the null (CURN) hypothesis. While the data are fixed, the models are uncertain and vary across posterior samples, so we adopt a noise-marginalized approach [28, 29]. For each posterior-sample CURN universe, we compute the three detection statistics and evaluate their false-alarm probabilities analytically using the appropriate generalized χ^2 distribution [32, 33]. We then form a histogram of the resulting p values.

We first discuss the NPMV statistic, whose posterior p -value histogram is shown in Fig. 3. The mean and median false-alarm probabilities are $p = 3.4 \times 10^{-3}$ and $p = 7.2 \times 10^{-4}$ for free γ_{gw} and $p = 2.9 \times 10^{-3}$ and $p = 9.0 \times 10^{-4}$ for fixed $\gamma_{gw} = 13/3$. Respectively, these correspond to 2.7σ , 3.2σ , 2.8σ , and 3.1σ equivalent Gaussian significances. The most likely range is shown in Fig. 3 as the band that contains 68% of the posterior points about the median. These correspond to significances in the range from $2.5 - 3.8\sigma$ for free γ_{gw} and $2.6 - 3.7\sigma$ for $\gamma_{gw} = 13/3$.

statistic	significance	mean	median	68% range	95% range
OS	σ -units:	4.0	4.5	(4.0, 5.1)	(3.4, 5.6)
	$-\log_{10} p$:	4.4	5.5	(4.4, 6.7)	(3.5, 8.0)
NP	σ -units:	2.6	3.1	(2.5, 3.7)	(1.9, 4.2)
	$-\log_{10} p$:	2.4	3.0	(2.2, 3.9)	(1.5, 4.9)
NPMV	σ -units:	2.7	3.2	(2.5, 3.8)	(2.0, 4.5)
	$-\log_{10} p$:	2.5	3.1	(2.3, 4.2)	(1.6, 5.4)

TABLE III. Posterior distributions of the false-alarm probability p for γ_{gw} free. OS is the traditional “optimal” statistic, NP is the Neyman–Pearson statistic, and NPMV is the robust NP statistic. Ranges are centered about the median, and p -values are also translated into “equivalent- σ ” units.

The corresponding histograms for the NP and OS false-alarm probabilities p have a similar appearance, so are not shown. Instead, we summarize the most important information for all three statistics in Table III. None has a mean false-alarm probability p small enough to exceed the 5σ threshold for confident detection [12]. However, it is notable that our analysis yields a traditional OS detection significance of $\approx 4.0\sigma$, which is substantially higher than the $\approx 3.2\sigma$ significance reported by NG [34]. This indicates that the “direct data combination” method is working as would be expected in the presence of an SGWB.

Another way to quantify detection confidence is through the *Bayes factor* (BF), defined as the ratio of the *evidence* for the HD model to that for the CURN model [12]. The evidence is the likelihood marginalized over the prior [57]. In our case, evaluating this marginalization integral is challenging because the parameter space is high-dimensional: $4 \times 121 + 2 = 486$ dimensions when γ_{gw} is free (or 485 when γ_{gw} is fixed to 13/3). To compute the evidence, we use the generalized stepping-stone sampling method [58–60], which progressively “broadens” the sharply peaked likelihood using $K = 8$ chains with $K - 1 = 7$ steps, while also restricting the integration region in parameter space.

This yields $\ln(\text{BF}) = 10.5 \pm 1.0$, corresponding to $\text{BF} \approx 40000$, which is substantially larger than the $\text{BF} \approx 200$ previously reported by NG [9]. For a one-dimensional Gaussian random variable, this BF corresponds to a significance of $\sqrt{2 \ln(\text{BF})} \sigma \approx 4.6\sigma$ [29, Eq. (8)], which is below that required for a confident detection.

Another detection confidence test is to estimate the

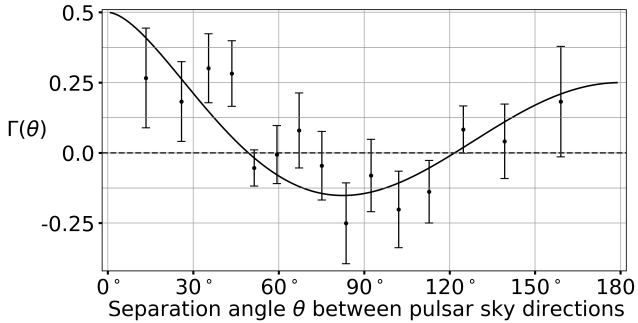


FIG. 4. Reconstruction of the mean correlation between pulsar pairs as a function of angular separation, compared to the Hellings and Downs (HD) prediction (2). The vertical bars indicate the uncertainties in the estimates of the means.

inter-pulsar correlation pattern from the data [12]. The mean correlation Γ_{ab} between pulsars a and b arising from an SGWB should follow the HD prediction [2, 25, 26]

$$\Gamma_{ab} \equiv \frac{1}{2}(1+\delta_{ab}) + \frac{3}{4}(1-\cos\theta) \left[\ln\left(\frac{1-\cos\theta}{2}\right) - \frac{1}{6} \right]. \quad (2)$$

Here, θ is the angle between unit vectors \hat{n}_a and \hat{n}_b pointing from Earth to pulsars a and b , so $\cos\theta = \hat{n}_a \cdot \hat{n}_b$. This pattern is shown in Fig. 4 as a function of θ . [The δ_{ab} in (2) doubles the correlation for two pulsars with spatial separation smaller than the GW wavelength [2]. It plays no role in the Fig. 4 comparison: the 15 angular bins contain only cross-pulsar pairs $a \neq b$, for which the Kronecker- δ vanishes.]

An optimal method for “reconstructing” the HD correlation from the data has been derived [61] but is not yet fully implemented [44]. So, our reconstruction is based on the same method [54] previously used by EPTA [7] and NG [9], as implemented in [62]. Fig. 4 shows the result for the 20480 free γ_{gw} CURN posterior samples.

Our HD reconstruction adopts the NG [9] choice of 15 angular bins. The $121 \times 120/2 = 7260$ pulsar pairs are divided equally: each bin contains 484 pairs. For each posterior sample, the correlations of the pulsar pairs are weighted as in [62], giving 20480 mean correlations μ and their variances σ_μ^2 for each bin. For each bin, we then construct and average 20480 different Gaussian probability distributions. The resulting 15 (posterior estimators of the) probability distributions of the correlation are sharply peaked. Fig. 4 shows their means (very close to medians) and standard deviations. The reconstruction matches the HD curve: the reduced χ^2 of 0.84 is consistent with normal statistical fluctuations (p -value 0.63 for 15 degrees of freedom).

Conclusion — We have conducted a search for a stochastic gravitational-wave background (SGWB) using data from five PTAs. The analysis is straightforward in the PTA context: we apply only minor adjustments to the pulsar noise models and discard a small fraction of

data. In essence, we repeat an established analysis using a larger dataset.

Our results provide the strongest evidence to date that an SGWB contributes to the observed pulsar pulse arrival-time fluctuations. However, the statistical significance of this evidence—assessed using multiple frequentist and Bayesian methods—remains too low to support a definitive detection.

Our use of existing data-analysis pipelines and infrastructures makes it straightforward to compare our results with those of the individual PTAs, but it has drawbacks. For example, these pipelines assume that, for a stationary process, the Fourier amplitudes in different frequency bins are statistically independent. While this is not strictly correct [61, see Conclusion], the resulting effects may be negligible or readily corrected [43]. Similarly, our reconstruction of the HD curve is suboptimal because the implementation of an optimal method [61] is still in progress [44].

As part of its upcoming data release, the IPTA is re-analyzing the five-PTA plus CPTA dataset to produce an IPTA-DR3 release (new `.par` and `.tim` files). If the primary outcome of this re-analysis is the adoption of common astrophysical models for the pulsars, then—per the arguments above—we expect an SGWB search of the five-PTA data to yield results consistent with ours. But if the re-analysis reveals that some data are incorrect and must be discarded, the results could differ. In this sense, the reliability of our conclusions depends on the correctness of the five existing PTA analyses.

We have deliberately kept this analysis as straightforward as possible and have not “iterated” it. This departs from standard practice in pulsar astronomy, where models—for example, pulsar timing parameters—are iteratively refit for improvement. Here, we avoid such iterative refinement and tuning of the full PTA search pipeline. Past experience with weak-signal detection in the LIGO context, as well as theoretical studies in the PTA context [11], suggests that such iteration can be misleading.

Because they are not public, we have not been able to include CPTA data [8] in our analysis. The CPTA data come from the Five-hundred-meter Aperture Spherical Telescope (FAST) in Guizhou Province, China. FAST is the world’s most sensitive radio telescope, and its data are of very high quality. Including them in future analyses would be both interesting and informative.

Note: the complete code used for this work will be posted publicly at the time of publication.

Acknowledgments — We thank Rutger van Haasteren for many useful conversations and discussions, for his encouragement with this project, and for his comments on various drafts of the manuscript. We also thank Stanislav Babak, Siyuan Chen, Colin Clark, Oliver Dodge, Boris Goncharov, Michael Kramer, Joseph Romano, and Michele Vallisneri for helpful feedback.

* wangwei.yu@aei.mpg.de
 † bruce.allen@aei.mpg.de

[1] S. R. Taylor, *Nanohertz Gravitational Wave Astronomy*, 1st ed. (CRC Press, Taylor & Francis Group, Boca Raton, 2021) see also arXiv:2105.13270 [astro-ph.HE], <https://arxiv.org/abs/2105.13270>.

[2] J. D. Romano and B. Allen, *Answers to frequently asked questions about the pulsar timing array Hellings and Downs curve*, Classical and Quantum Gravity **41**, 175008 (2024), arXiv:2308.05847.

[3] G. Agazie, A. Anumarlapudi, A. M. Archibald, P. T. Baker, B. Bécsy, L. Blecha, A. Bonilla, A. Brazier, P. R. Brook, S. Burke-Spoloar, et al., *The NANOGrav 15 yr Data Set: Constraints on Supermassive Black Hole Binaries from the Gravitational-wave Background*, The Astrophysical Journal Letters **952**, L37 (2023), arXiv:2306.16220.

[4] S. Burke-Spoloar, S. R. Taylor, M. Charisi, T. Dolch, J. S. Hazboun, A. M. Holgado, L. Z. Kelley, T. J. W. Lazio, D. R. Madison, N. McMann, et al., *The astrophysics of nanohertz gravitational waves*, The Astronomy and Astrophysics Review **27**, 5 (2019), arXiv:1811.08826 [astro-ph.HE].

[5] E. Phinney, *A Practical Theorem on Gravitational Wave Backgrounds*, arXiv preprint astro-ph/0108028 (2001).

[6] D. J. Reardon et al. (PPTA Collaboration), *Search for an Isotropic Gravitational-wave Background with the Parkes Pulsar Timing Array*, The Astrophysical Journal Letters **951**, L6 (2023), arXiv:2306.16215.

[7] J. Antoniadis et al. (EPTA and InPTA Collaborations), *The second data release from the European Pulsar Timing Array: III. Search for gravitational wave signals*, Astronomy & Astrophysics **678**, A50 (2023), arXiv:2306.16214.

[8] H. Xu et al. (CPTA Collaboration), *Searching for the Nano-Hertz Stochastic Gravitational Wave Background with the Chinese Pulsar Timing Array Data Release I*, Research in Astronomy and Astrophysics **23**, 075024 (2023), arXiv:2306.16216.

[9] G. Agazie et al. (NANOGrav Collaboration), *The NANOGrav 15 yr Data Set: Evidence for a Gravitational-wave Background*, The Astrophysical Journal Letters **951**, L8 (2023), arXiv:2306.16213.

[10] M. T. Miles, R. M. Shannon, D. J. Reardon, M. Bailes, D. J. Champion, M. Geyer, P. Gitika, K. Grunthal, M. J. Keith, M. Kramer, et al., *The MeerKAT Pulsar Timing Array: The first search for gravitational waves with the MeerKAT radio telescope*, Monthly Notices of the Royal Astronomical Society **536**, 1489 (2025), arXiv:2412.01153.

[11] R. van Haasteren, *Use model averaging instead of model selection in pulsar timing*, Monthly Notices of the Royal Astronomical Society: Letters **537**, L1 (2024), arXiv:2409.06050.

[12] B. Allen, S. Dhurandhar, Y. Gupta, M. McLaughlin, P. Natarajan, R. M. Shannon, E. Thrane, and A. Vecchio, *The International Pulsar Timing Array checklist for the detection of nanohertz gravitational waves* (2023), arXiv:2304.04767 [astro-ph.IM].

[13] J. M. Goldstein, J. Veitch, A. Sesana, and A. Vecchio, *Null-stream analysis of pulsar timing array data: localization of resolvable gravitational wave sources*, Monthly Notices of the Royal Astronomical Society **477**, 5447 (2018), arXiv:1712.03975.

[14] B. Perera, M. DeCesar, P. Demorest, M. Kerr, L. Lentati, D. Nice, S. Osłowski, S. Ransom, M. Keith, Z. Arzoumanian, et al., *The International Pulsar Timing Array: second data release*, Monthly Notices of the Royal Astronomical Society **490**, 4666 (2019), arXiv:1909.04534.

[15] J. G. Baier, J. S. Hazboun, and J. D. Romano, *A sensitivity curve approach to tuning a pulsar timing array in the detection era*, Class. Quant. Grav. **42**, 075008 (2025), arXiv:2409.00336 [astro-ph.HE].

[16] EPTA Collaboration, EPTA data set DR2new, 27.4.2023, commit be91c6be8623df1ab8b66d5e36281005c6ca6851 <https://gitlab.in2p3.fr/epta/epta-dr2/-/tree/master/EPTA-DR2/DR2new>. As this draft was being completed, we found that there is a later commit dated 23.8.2025 with hash 1506123cae38bd2fb88df53d28f87cdb87c2f389, but have not yet investigated the differences.

[17] InPTA Collaboration, InPTA data release 1, commit 2c400d51428abd59d6cf842cd8fe7c840e819d0d, <https://github.com/inpta/InPTA.DR1>.

[18] MPTA Collaboration, MPTA 4.5-yr data set, <https://docs.datacentral.org.au/meerkat-pulsar-timing-array/45-year-accessing-the-data/>.

[19] NANOGrav Collaboration, NANOGrav data set 15yr, v1.0.0, <https://zenodo.org/records/7967585>.

[20] PPTA Collaboration, PPTA data release 3, <https://data.csiro.au/collection/csiro%3A59381v1> (2023), cSIRO Data Collection.

[21] R. van Haasteren and W.-W. Yu, *The direct combination method for PTA data analysis* (2025), work in progress, https://github.com/vhaasteren/metapulsar/blob/main/docs/METHOD_DESCRIPTION.md.

[22] R. van Haasteren and W.-W. Yu, *MetaPulsar* (2025), zenodo, <https://doi.org/10.5281/zenodo.1762664>.

[23] J. A. Ellis, M. Vallisneri, S. R. Taylor, and P. T. Baker, *Enterprise: Enhanced Numerical Toolbox Enabling a Robust Pulsar Inference Suite*, Astrophysics Source Code Library, ascl (2019).

[24] NANOGrav Discovery Pipeline, <https://github.com/nanograv/discovery> (2025), accessed: 2025-11-10.

[25] R. W. Hellings, *Pulsar timing and gravitational waves*, in *Relativistic Gravitational Experiments in Space: proceedings of NASA Workshop, Annapolis, Maryland, June 28-30, 1988*, NASA Conference Publication, Vol. 3046 (1989) pp. 93–97.

[26] B. Allen, *Variance of the Hellings-Downs correlation*, Physical Review D **107**, 043018 (2023), arXiv:2205.05637.

[27] R. van Haasteren, B. Allen, and J. D. Romano, *Optimal robust detection statistics for pulsar timing arrays* (2025), arXiv:2509.06489 [astro-ph.IM].

[28] S. J. Vigeland, K. Islo, S. R. Taylor, and J. A. Ellis, *Noise-marginalized optimal statistic: A robust hybrid frequentist-Bayesian statistic for the stochastic gravitational-wave background in pulsar timing arrays*, Physical Review D **98**, 044003 (2018), arXiv:1805.12188.

[29] M. Vallisneri, P. M. Meyers, K. Chatzioannou, and A. J. Chua, *Posterior predictive checking for gravitational-wave detection with pulsar timing arrays. I. the optimal statistic*, Physical Review D **108**, 123007 (2023), arXiv:2306.05558.

[30] N. J. Cornish and L. Sampson, *Towards robust gravitational wave detection with pulsar timing arrays*, Physical Review D **93**, 104047 (2016), arXiv:1512.06829.

[31] S. Taylor, L. Lentati, S. Babak, P. Brem, J. Gair, A. Sesana, and A. Vecchio, *All correlations must die: Assessing the significance of a stochastic gravitational-wave background in pulsar timing arrays*, Physical Review D **95**, 042002 (2017), arXiv:1606.09180.

[32] R. van Haasteren, *Calculation of p-values for quadratic statistics in pulsar timing arrays*, Physical Review D **112**, 103009 (2025), arXiv:2506.10811 [astro-ph.IM].

[33] J. S. Hazboun, P. M. Meyers, J. D. Romano, X. Siemens, and A. M. Archibald, *Analytic distribution of the optimal cross-correlation statistic for stochastic gravitational-wave-background searches using pulsar timing arrays*, Physical Review D **108**, 104050 (2023), arXiv:2305.01116.

[34] *The nanograv 15 yr dataset: Posterior predictive checks for gravitational-wave detection with pulsar timing arrays*, Phys. Rev. D **111**, 042011 (2025).

[35] J. Antoniadis, S. Babak, A.-S. B. Nielsen, C. Bassa, A. Berthureau, M. Bonetti, E. Bortolas, P. Brook, M. Burgay, R. Caballero, *et al.*, *The second data release from the European Pulsar Timing Array-I. The dataset and timing analysis*, Astronomy & Astrophysics **678**, A48 (2023), arXiv:2306.16224.

[36] P. Tarafdar, K. Nobleson, P. Rana, J. Singha, M. Krishnakumar, B. C. Joshi, A. K. Paladi, N. Kolhe, N. D. Batra, N. Agarwal, *et al.*, *The Indian Pulsar Timing Array: First data release*, Publications of the Astronomical Society of Australia **39**, e053 (2022), arXiv:2206.09289.

[37] M. T. Miles, R. M. Shannon, D. J. Reardon, M. Bailes, D. J. Champion, M. Geyer, P. Gitika, K. Grunthal, M. J. Keith, M. Kramer, *et al.*, *The MeerKAT Pulsar Timing Array: the 4.5-yr data release and the noise and stochastic signals of the millisecond pulsar population*, Monthly Notices of the Royal Astronomical Society **536**, 1467 (2025), arXiv:2412.01148.

[38] G. Agazie, M. F. Alam, A. Anumarlapudi, A. M. Archibald, Z. Arzoumanian, P. T. Baker, L. Blecha, V. Bonidie, A. Brazier, P. R. Brook, *et al.*, *The NANOGrav 15 yr data set: observations and timing of 68 millisecond pulsars*, The Astrophysical Journal Letters **951**, L9 (2023), arXiv:2306.16217.

[39] A. Zic, D. J. Reardon, A. Kapur, G. Hobbs, R. Mandow, M. Curylo, R. M. Shannon, J. Askew, M. Bailes, N. R. Bhat, *et al.*, *The Parkes Pulsar Timing Array third data release*, Publications of the Astronomical Society of Australia **40**, e049 (2023), arXiv:2306.16230.

[40] G. Hobbs, R. Edwards, and R. Manchester, *TEMPO2, a new pulsar timing package. 1. Overview*, Mon. Not. R. Astron. Soc. **369**, 655 (2006), arXiv:astro-ph/0603381.

[41] B. Goncharov, S. Sardana, A. Sesana, S. M. Tomson, J. Antoniadis, A. Chalumeau, D. J. Champion, S. Chen, E. F. Keane, K. Liu, *et al.*, *Reading signatures of supermassive binary black holes in pulsar timing array observations*, Nature Communications **16**, 9692 (2025), arXiv:2409.03627.

[42] M. Blondel, Q. Berthet, M. Cuturi, R. Frostig, S. Hoyer, F. Llinares-López, F. Pedregosa, and J.-P. Vert, *Efficient and modular implicit differentiation*, Advances in neural information processing systems **35**, 5230 (2022), arXiv:2105.15183.

[43] M. Crisostomi, R. van Haasteren, P. M. Meyers, and M. Vallisneri, *Beyond diagonal approximations: improved covariance modeling for pulsar timing array data analysis* (2025), arXiv:2506.13866 [astro-ph.IM].

[44] B. Allen, A. L. von Blanckenburg, and K. D. Olum, *Pulsar timing array analysis in a Legendre polynomial basis* (2025), arXiv:2510.05913 [gr-qc].

[45] D. Nice, P. Demorest, I. Stairs, R. Manchester, J. Taylor, W. Peters, J. Weisberg, A. Irwin, N. Wex, and Y. Huang, *TEMPO: Pulsar timing data analysis*, Astrophysics Source Code Library, ascl:1509.002 (2015).

[46] J. Luo, S. Ransom, P. Demorest, P. S. Ray, A. M. Archibald, M. Kerr, R. J. Jennings, M. Bachetti, R. van Haasteren, C. A. Champagne, J. Colen, C. Phillips, J. Zimmerman, K. Stovall, M. T. Lam, *et al.*, *PINT: A modern software package for pulsar timing*, Astrophys. J. **911**, 45 (2021), arXiv:2012.00074 [astro-ph.IM].

[47] J. Bradbury, R. Frostig, P. Hawkins, M. J. Johnson, C. Leary, D. Maclaurin, G. Necula, A. Paszke, J. VanderPlas, S. Wanderman-Milne, and Q. Zhang, *JAX: composable transformations of Python+NumPy programs* (2018).

[48] R. M. Neal *et al.*, *MCMC using Hamiltonian dynamics*, Handbook of Markov Chain Monte Carlo **2**, 2 (2011), arXiv:1206.1901.

[49] M. D. Hoffman, A. Gelman, *et al.*, *The No-U-Turn sampler: adaptively setting path lengths in Hamiltonian Monte Carlo.*, J. Mach. Learn. Res. **15**, 1593 (2014), arXiv:1111.4246.

[50] D. Phan, N. Pradhan, and M. Jankowiak, *Composable effects for flexible and accelerated probabilistic programming in numpyro*, arXiv preprint arXiv:1912.11554 (2019).

[51] E. Bingham, J. P. Chen, M. Jankowiak, F. Obermeyer, N. Pradhan, T. Karaletsos, R. Singh, P. A. Szerlip, P. Horsfall, and N. D. Goodman, *Pyro: Deep universal probabilistic programming*, J. Mach. Learn. Res. **20**, 28:1 (2019), arXiv:1810.09538.

[52] M. Betancourt, *A conceptual introduction to Hamiltonian Monte Carlo*, arXiv preprint arXiv:1701.02434 (2017).

[53] J. Ellis and R. van Haasteren, *jellis18/ptmcmc sampler: Official release* (2017).

[54] B. Allen and J. D. Romano, *Hellings and Downs correlation of an arbitrary set of pulsars*, Physical Review D **108**, 043026 (2023), arXiv:2208.07230.

[55] G. Agazie, J. Antoniadis, A. Anumarlapudi, A. M. Archibald, P. Arumugam, S. Arumugam, Z. Arzoumanian, J. Askew, S. Babak, M. Bagchi, and *et al.* (International Pulsar Timing Array), *Comparing Recent Pulsar Timing Array Results on the Nanohertz Stochastic Gravitational-wave Background*, Astrophys. J. **966**, 105 (2024), arXiv:2309.00693 [astro-ph.HE].

[56] C. Pernet, *Null hypothesis significance testing: a short tutorial*, F1000Research **4**, 621 (2016).

[57] H. Jeffreys, *Theory of Probability*, 3rd ed., International Series of Monographs on Physics (Clarendon Press, Oxford, 1961).

[58] E. M. Zahraoui, P. Maturana-Russel, W. van Straten, R. Meyer, and S. Gulyaev, *Generalized stepping-stone sampling: efficient marginal likelihood estimation in gravitational wave analysis of pulsar timing array data*, Monthly Notices of the Royal Astronomical Society **540**, 3818 (2025), arXiv:2411.14736 [astro-ph.IM].

[59] E. M. Zahraoui, P. Maturana-Russel, W. van Straten, R. Meyer, and S. Gulyaev,

<https://github.com/apokryphav1/gss-estimator/tree/main> (2024).

[60] The code we used in the paper will become a pull request in *Discovery*.

[61] B. Allen and J. D. Romano, *Optimal reconstruction of the Hellings and Downs correlation*, Physical Review Letters **134**, 031401 (2025), arXiv:2407.10968.

[62] NANOGrav Collaboration, NANOGrav 15-year stochastic analysis repository, https://github.com/nanograv/15yr_stochastic_analysis/blob/main/tutorials/optimal_statistic_covariances.py (2023), file: *tutorials/optimal_statistic_covariances.py*, commit: 14ed645b7d26be788340036ded29b3c66286e29c.